

Nanoencapsulation of hydroxytyrosol in chitosan crosslinked with sodium bisulfate tandem ultrasonication: Techno-characterization, release and antiproliferative properties

Touseef Ahmed Wani^a, F.A. Masoodi^{a,*}, Rehana Akhter^a, Towseef Akram^b, Adil Gani^a, Nadeem Shabir^b

^a Department of Food Science and Technology, University of Kashmir, Hazratbal, Srinagar 190006, Jammu and Kashmir, India

^b Division of Biotechnology, Faculty of Veterinary Sciences and Animal Husbandry, Sher-e-Kashmir University of Agricultural Sciences and Technology-Kashmir, Shuhama 191202, Jammu and Kashmir, India

ARTICLE INFO

Keywords:

Nanoencapsulation
Hydroxytyrosol
Chitosan
Ionic gelation
Targeted delivery

ABSTRACT

This research includes production of chitosan nanocapsules through ionic gelation with sodium bisulfate for nanoencapsulation of hydroxytyrosol (HT) using ultrasonication in tandem. The resulting nanocapsules encapsulating HT were analyzed for particle size, ζ -potential, packaging characteristics, FESEM, ATR-FTIR, XRD, DSC, *in vitro* release, antioxidant potential and antiproliferative properties. The nanocapsules (size 119.50–365.21 nm) were spherical to irregular shaped with positive ζ -potential (17.50–18.09 mV). The encapsulation efficiency of 5 mg/g HT (HTS1) and 20 mg/g HT (HTS2) was 77.13% and 56.30%, respectively. The nanocapsules were amorphous in nature with 12.34% to 15.48% crystallinity and crystallite size between 20 nm and 27 nm. Formation of nanocapsules resulted in increasing the glass transition temperature. HTS2 delivered 67.12% HT (HTS1 58.89%) at the end of the simulated gastrointestinal digestion. The nanoencapsulated HT showed higher antioxidant and antiproliferative (against A549 and MDA-MB-231 cancer cell lines) properties than the free HT.

1. Introduction

Chitosan is produced after the deacetylation of chitin harvested from crustacean shells [32]. Chemically, chitosan is a polysaccharide copolymer of β -(1–4)-linked D-glucosamine and N-acetyl-D-glucosamine having linear linkages. Being the second largest available biopolymer in nature, the applications of chitosan have been tremendously explored in the food [53], packaging [8], pharmaceutical [24,27], and agricultural [56] industries, among others. Chitosan forms self assembled gel at a concentration of 0.03 mg/mL after heating at 90 °C for 30 min [58]. However, the application of the self assembled gels for thermolabile molecules is offset by the requirement of a high gelation temperature for a long time. Contrary to the self assembly, the ionic gelation process of chitosan is highly efficient, effective, controllable and convenient [21]. The electrostatic interaction of the positively charged chitosan with a negatively charged polymer/matrix leads to the formation of nanosized cores [48] that can accommodate the active ingredients for various food and pharmaceutical applications.

Hydroxytyrosol (4-(2-Hydroxyethyl)-1,2-benzenediol) is one of the

most potent phenolic compounds having the European Food Safety authority (EFSA) approved health implications [19]. Over the years, researchers from around the world have reported a wide range of health implications and disease preventing potential of HT *in vitro* and *in vivo*. HT has been explored against a number of health complications including diabetes, inflammation, nervous disorders, angiogenesis, oxidative stress, heavy metal toxicity, hemolysis, LDL oxidation, muscle damage, and nephrotoxicity with positive outcomes [57]. HT has demonstrated antiproliferative and pro-apoptotic activities against Caco-2, HT-29 [15] and prostate (LNCaP and C4-2) cancer cells [62]. Irrespective of its high bioactive potential, HT has poor bioavailability evident from its pharmacokinetics post consumption that include area under the curve (5.3 ng h/mL), maximum plasma concentration (4.4 ng/mL), time to reach the maximum plasma concentration (0.25 h), elimination rate constant (0.25/h), and elimination half-life (2.8 h) [42]. This necessitates the development of delivery vehicles for HT that could not only protect it against the deleterious reactions in the alimentary canal but also release it progressively in a delayed fashion. The previous reports on the encapsulation of HT include the use of emulsion systems

* Corresponding author.

E-mail address: masoodi_fa@yahoo.co.in (F.A. Masoodi).

<https://doi.org/10.1016/j.ultsonch.2021.105900>

Received 25 November 2021; Received in revised form 23 December 2021; Accepted 27 December 2021

Available online 28 December 2021

1350-4177/© 2021 Published by Elsevier B.V. This is an open access article under the CC BY-NC-ND license (<http://creativecommons.org/licenses/by-nc-nd/4.0/>).

[23,11] (Cofrades et al., 2017), liposomes [9], and ethyl cellulose microparticles [43].

Research over the years has revealed the possibility of many different biomaterials to ionically gel with chitosan polymer including collagen peptide [4], adenosine triphosphate [44], phytic acid [13], poly (sodium 4-styrene sulfonate) and sodium tripolyphosphate [28] resulting in the formation of nanocapsules. However, to the best of our knowledge, there is no published literature on the detailed account of ionic gelation of chitosan with inorganic substances that are generally recognized as safe (GRAS) for human consumption by the United States Food and Drug Administration (FDA). One of the most important anionic substances with GRAS status is disodium hydrogen phosphate. However, our preliminary research on disodium hydrogen phosphate revealed that it does not take part in ionic gelation with chitosan at all. On the other hand, sulfate anions including sodium sulfate and potassium bisulfate, among others take part in ionic gelation with chitosan. Sodium sulfate has been used for precipitation-coacervation of chitosan to yield nanoparticles having high protein loading efficiencies [31], precipitation/coacervation of chitosan to yield nanocapsules for efficient loading of ovalbumin [30], crosslinking of chitosan into microspheres for encapsulating the cell protein antigen of *Helicobacter pylori* [34], crosslinking of chitosan to yield nontoxic *in situ* injectable hydrogels for sustained release of curcumin [50], layer-by-layer self-assembly of chitosan into microcapsules for the spontaneous loading of heparin [47], and precipitation of chitosan for the formulation of microspheres loading different steroidal anti-inflammatory drugs [7].

However, these anionic substances are not recognized as safe by the U.S FDA. Therefore, the present research was based on ionic gelation of chitosan polymer with sodium bisulfate producing chitosan nanoparticles/nanocapsules for possible applications in nanoencapsulation using the ultrasonication process. Ultrasonication is one of the physical methods employed for encapsulation of bioactive compounds in different polymeric materials [33]. The high intensity ultrasound waves with frequencies in the range of 20 to 100 kHz produce cavitation, which is responsible for biomaterial surface destruction and internalization of bioactive compounds from the medium into the polymeric material [33,49]. Sodium bisulfate is commonly used as a food additive in different bakery products, meat and poultry. Being reported for the first time, it would be interesting to know the physical, chemical, structural, antioxidant and antiproliferative properties of the chitosan nanoparticles encapsulating HT.

2. Materials and methods

2.1. Chemicals and reagents

Chitosan (Moisture 11.5% & Degree of deacetylation \geq 75%) and sodium bisulfate (\geq 99%) were purchased from HiMedia India. Dulbecco's Modified Eagle Media - high glucose (DMEM), Dulbecco's Buffered Saline (DPBS) and Hydroxytyrosol (\geq 98%) were purchased from Sigma Aldrich. All other chemicals and reagents used in this research were analytical grade and purchased either from either Sigma Aldrich or HiMedia India.

2.2. Nanoencapsulation of HT

Chitosan solution (1.5% w/v) was prepared by dissolving chitosan in 1% (v/v) glacial acetic acid solution. After complete dissolution, the solution was centrifuged at 4000 rpm for 5 min to clear any heterogeneous impurities in the solution. Simultaneously, 0.75% (w/v) solution of sodium bisulfate was prepared in double distilled water. A 1 mg/mL solution of HT was prepared in double distilled water and added drop by drop to chitosan solution under continuous stirring using a magnetic stirrer. The stirring was continued for 10 min before adding the sodium bisulfate solution slowly into the chitosan-HT mixture and the stirring was continued for 1 h at ambient temperature (25 ± 1 °C). Finally, the

solution containing HT nanocapsules was ultrasonicated for 5 min at 40 kHz and frozen to -18 °C before subjecting it to freeze drying (BIOBASE, BK-FD10P). The control sample was prepared without including HT in the nanocapsules. The HTS1 and HTS2 samples included 5 mg/g and 20 mg/g of HT in the finally dried nanoencapsulated powders, respectively. All the freeze dried samples were sealed in air tight containers and stored at -18 °C till further analysis.

2.3. Particle size distribution and ζ -potential

The powder material (10 mg/mL) was suspended in 1% acetic acid solution and sonicated for 30 min at 35 kHz. The dynamic light scattering (DLS) measurements including particle size distribution and ζ -potential were taken at 90° spectral angle in Litesizer 500 (Anton Paar) at ambient temperature (25 ± 1 °C).

2.4. Attenuated total reflectance-fourier transform infrared spectroscopy

Attenuated total reflectance-fourier transform infrared spectroscopy (ATR-FTIR) of the nanocapsules was performed in the wavelength range of $450\text{--}4000$ cm^{-1} using an ATR-FTIR spectrophotometer (CARY 630, Agilent Technologies, USA).

2.5. X-ray diffraction

The X-ray diffraction (XRD) of the nanocapsules was performed on a diffractometer (Rigaku, SmartLab 3 kW-BD67000130, Tokyo, Japan). The parameter settings of the equipment include 40 kV and 30 mA. The scanning of the samples was performed through diffraction angle of 5° to 90° at the rate of $5^\circ/\text{min}$. The relative crystallinity (RC) of the samples was calculated by using equation (i).

$$\text{RC}(\%) = \frac{A_{\text{cr}}}{A_{\text{cr}} + A_{\text{am}}} \times 100$$

Where, A_{cr} and A_{am} included area under the crystalline and amorphous peaks of the diffractogram, respectively.

Size of the crystallites was calculated using the Hall-Williamson equation (ii).

$$D = \frac{k\lambda\eta\sin\theta}{\beta\cos\theta}$$

Where, D is the crystallite size, β is the full width half maximum (FWHM) of the diffraction peak, k is the shape factor ($=0.89$), λ is the wavelength of the X-ray radiation, η is the strain in the crystallite and θ is Bragg's diffraction angle.

2.6. Differential scanning calorimetry

The thermal characterization of the samples was performed using the differential scanning calorimetry (DSC) equipment (Mettler-Toledo, Staresystems, Switzerland). Briefly, the sample (5 mg) was loaded in a platinum crucible, sealed properly and submitted to the equipment chamber for analysis. The temperature of the system was programmed to rise from 25 °C to 350 °C at the rate of 10 °C/min in an inert atmosphere under a continuous supply of nitrogen flowing at the rate of 40 mL/min. Interpretation of data into the characteristic thermal parameters including onset temperature (T_o), peak temperature (T_p), completion temperature (T_c) and enthalpy (ΔH) was performed after analyzing the data in the system software of the instrument.

2.7. Field emission scanning electron microscopy

The morphological properties of the powder samples were evaluated through field emission scanning electron microscopy (FESEM) (GeminiSEM 500 8203017193, UK/GB). The samples were mounted on the

grid and coated with gold before taking the FESEM images at 30000x magnification.

2.8. Packing characteristics of nanocapsules

2.8.1. Theoretical loading capacity

The theoretical loading capacity (LCT) of the wall material for HT was calculated using the equation (iii).

$$\text{LCT}(\%) = \frac{\text{Amount of HT added}}{\text{Amount of wall material}} \times 100$$

2.8.2. Encapsulation efficiency

The encapsulation efficiency (EE) of HT encapsulated nanocapsules was performed according to the method described by Ahmad and Gani [2] with slight modifications. Briefly, 100 mg nanoencapsulated powder was suspended in 30 mL of 10% ethanol followed by centrifugation at 4000 rpm for 10 min. The supernatant was discarded followed by addition of 5 mL of 10% ethanol for resuspending the mixture and was sonicated at 35 kHz for 1 h. The mixture was centrifuged at 4000 rpm for 10 min and the spectrophotometric absorbance (ependorf Biospectrometer 6135D0701977, S-W-Version- 4.3.5.0) of the supernatant was taken at 280 nm. The quantification of HT was performed from the standard calibration curve of the pure compound ($y = 0.012x - 0.000$; $R^2 = 0.977$) using the equation (iv).

$$X = \frac{A}{\epsilon L}$$

Where, X is concentration, A is absorbance at 280 nm, ϵ is the molar absorptivity coefficient and L is path length of the cuvette.

Finally, the EE was calculated using the equation (v).

$$\text{EE}(\%) = \frac{\text{Amount of HT encapsulated}}{\text{Amount of HT added}} \times 100$$

2.8.3. Loading capacity

The loading capacity (LC) of the wall material for HT was calculated according to McClements and Li [38] using the equation (vi).

$$\text{LC}(\%) = \frac{\text{Amount of HT encapsulated}}{\text{Amount of wall material}} \times 100$$

2.9. In vitro release behavior

2.9.1. Gastric digestion

In order to mimic the gastric digestion, the encapsulated powder was digested in simulated gastric juice (SGJ) prepared from porcine pepsin as per the method described by Feng et al. [22]. Briefly, 0.9 g NaCl and 0.15 g pepsin was dissolved in 0.01 mL HCl and the pH was adjusted to 2.0 using 0.1 M HCl. The sample powder (100 mg) was added to 10 mL of SGJ and allowed to incubate in the dark for 1 h at 37 °C with intermittent shaking. Sampling for the release of HT was done periodically after 30 min. and 1 h. Quantification of HT released from the nanocapsules was performed by using the equation (iv). After the completion of gastric digestion, the mixture was centrifuged at 4000 rpm for 5 min to recover the sample pellet for the subsequent intestinal digestion.

2.9.2. Intestinal digestion

The intestinal digestion of the encapsulated powder was performed in simulated intestinal juice (SIJ). Briefly, 0.3 g pancreatin and 1.0 g bile salt was dissolved in 100 mL phosphate buffered and the pH was adjusted to 7.5. The pellets recovered from gastric digestion were dispersed in 10 mL of SIJ and incubated in the dark for 2 h at 37 °C with intermittent shaking. In order to check the release of HT, periodic sampling was performed after each hour. The HT released from the nanocapsules during the intestinal digestion was quantified by using the equation (iv).

2.10. Antioxidant properties

2.10.1. Sample preparation

The nanocapsules were subjected to simulated gastrointestinal digestion in order to validate the effect of the encapsulation process. Briefly, the sample powder (600 mg) was added to 3 mL of SGJ and allowed to incubate in the dark for 1 h at 37 °C with intermittent shaking. Following gastric digestion, 3 mL of SIJ was also added to it and incubated in the dark for 2 h at 37 °C with intermittent shaking. The mixture was centrifuged at 4000 rpm for 10 min and the supernatant recovered was stored at -18 °C till further analysis. For comparison, free HT equal to the concentration used in HTS2 was also subjected to *in vitro* digestion.

2.10.2. 1,1-diphenyl-2-picrylhydrazyl (DPPH) radical scavenging activity

The DPPH radical scavenging activity was performed according to the method described by Matthus [37]. Briefly, methanol (2720 μ L) was added to the sample (80 μ L) before adding the DPPH solution (0.05%, 200 μ L). The contents were mixed thoroughly in a vortex shaker before allowing the reaction mixture to incubate for 30 min. in the dark at ambient temperature. Spectrophotometric absorbance was measured at 515 nm and the results were expressed as inhibition percent as described by the equation (vii).

$$\text{Inhibition}(\%) = \left(1 - \frac{\text{Absorbance of sample}}{\text{Absorbance of control}} \right) \times 100$$

2.10.3. Lipid peroxidation inhibition

The lipid peroxidation inhibition (LPI) was performed according to the method described by Wright, Colby, & Miles [59]. Briefly, a reaction mixture (2 mL) containing linoleic acid (1 mL), ferric nitrate (20 mM, 0.2 mL), ascorbic acid (200 mM, 0.2 mL) and hydrogen peroxide (300 mM, 0.2 mL) was added to the sample (100 μ L) and mixed thoroughly in a vortex shaker. The reaction mixture was incubated for 1 h at 37 °C followed by stopping the reaction using trichloroacetic acid (10% w/v, 1 mL) and thiobarbituric acid (10% w/v, 1 mL). The reaction mixture was again incubated for 20 min at 100 °C followed by centrifugation at 5000 rpm for 10 min. The spectrophotometric absorbance was measured at 535 nm and the results were expressed as inhibition percent as described by the equation (vii).

$$\text{Inhibition}(\%) = \left(1 - \frac{\text{Absorbance of sample}}{\text{Absorbance of control}} \right) \times 100$$

2.11. Antiproliferative properties

Antiproliferative properties of the nanoencapsulated HT was evaluated using the MTT reagent (3-(4,5-dimethylthiazol-2-yl)-2,5-diphenyltetrazolium bromide) against two cancer cell lines including adenocarcinomic human alveolar epithelial cells (A549) and human breast cancer cells (MDA-MB-231). The cells were cultured in Dulbecco's Modified Eagle Media - high glucose (DMEM) containing 5 % FBS + 0.1% penicillin and streptomycin. The cells were cultured in 96 well plates and incubated in a humidified chamber (Galaxy 170S, Eppendorf, Hamburg, Germany) at 37 °C and 5% CO₂. After 60–70 % confluency of the adherent cells, the media was removed. Then the wells were treated with 100 μ L DMEM (5 % FBS + 0.1% penicillin and streptomycin) containing the compounds at 0 to 6 μ g/mL in triplicates. To determine the antiproliferative properties at 24, 48 and 72 h post treatment (hpt), plates were incubated (37 °C and 5% CO₂) for 24, 48 and 72 h, respectively. After incubation for 24 h, media in the wells was aspirated and cells were washed two times with DPBS. Then 100 μ L of MTT reagent in DMEM (0.5 mg/mL) was added to the wells. After incubation for 4 h, 100 μ L of solubilizing solution (10 % Sodium dodecyl sulfate in 0.01 M HCl) was added and kept overnight to dissolve formazan crystals. These plates were then checked for optical density (OD) at 570 nm in a

multimode microplate reader (Biotek, Cytation™ 3, Winooski, VT, USA). Same procedure was followed for 48 and 72 hpt. Control wells (0 % compound) and blank wells (without cells) were utilized for calculating the cell viability by using the equation (ix).

$$\text{Cellviability}(\%) = \frac{\text{Sample absorbance} - \text{Blank absorbance}}{\text{Control absorbance} - \text{Blank absorbance}} \times 100$$

2.12. Statistical analysis

The data presented are means of triplicate determinations and were compared for the analysis of variance (ANOVA) through SPSS statistical software (IBM Statistics 21.0, Chicago, IL, USA) using the Duncan's test ($P \leq 0.05$) at 5% level of significance. Microsoft excel was used for making the histograms. The graphing software (OriginPro 8.5) was employed to plot the data into the graphical representations. The IC₅₀ for all the antiproliferative measurements was calculated using AAT Bioquest, Inc. online (<https://www.aatbio.com/tools/ic50-calculator>) accessed in March 2021.

3. Results and discussion

3.1. Particle size distribution and ζ -potential

The results of particle size analysis and ζ -potential of HT nanocapsules are provided in Table 1. The smallest particle size was found in the control nanocapsules (119.50 nm), which increased significantly ($P \leq 0.05$) upon increasing the concentration of HT in the encapsulation process. The polydispersity index of the nanocapsules ranged between 35% and 38%. The smaller polydispersity index indicates the higher level of control over the process of nanocapsule formation [1]. The nanodimensional size and smaller polydispersity indices in the different nanocapsules formed could be because of the ultrasonic cavitation process that maintains a similar set of particles in the solution [25]. However, aggregated nanoparticles still persist because of negligible impact of nanoparticles on the process of cavitation [60]. The zeta potential of the nanocapsules varied between 17.50 mV and 18.09 mV with insignificant ($p \geq 0.05$) difference among the nanocapsules. Because of the presence of $-\text{NH}_3^+$ (-ammoniumyl) groups on the surface, a high positive zeta potential (56.48 ± 3.25 mV) is characteristic to chitosan polymer [46,55]. Upon ionic gelation with sodium bisulfate, the zeta potential of the nanocapsules is reduced. The probable reason for the similar zeta potential in all the nanocapsules is the same proportion of the chitosan polymer and sodium bisulfate used in the ionic gelation process. The high zeta potential values of the nanocapsules formed indicate their better stability to aggregation into still larger particles due to the repulsive forces exerted by the positive surface charge of the particles [3].

3.2. Packing characteristics of nanocapsules

The packing characteristics of chitosan nanocapsules encapsulating

Table 1
Particle size, zeta potential, and packaging characteristics of HT nanocapsules.

Parameter	Particle size (nm)	PI (%)	ζ -potential (mV)	LCT (%)	EE (%)	LC (%)
Control	119.50 ± 47.24 ^a	35	17.50 ± 0.34 ^a	--	--	--
HTS1	323.35 ± 80.79 ^b	37	18.09 ± 0.52 ^a	0.30 ± 0.00 ^a	77.13 ± 11.45 ^b	0.14 ± 0.02 ^a
HTS2	365.21 ± 134.00 ^b	38	17.68 ± 0.60 ^a	1.41 ± 0.00 ^b	56.30 ± 8.11 ^a	0.56 ± 0.08 ^b

Values are presented as Mean ± Standard deviation.

Means with different superscripts are significantly ($p \leq 0.05$) different.

PI = Polydispersity index, LCT = Theoretical loading capacity, EE = Encapsulation efficiency and LC = Loading capacity.

HT including theoretical loading capacity (LCT), encapsulation efficiency (EE) and loading capacity (LC) are provided in Table 1. As one of the most powerful bioactive compounds discovered so far, we encapsulated HT at two different concentrations in chitosan nanoparticles ionically crosslinked with sodium bisulfate. In the treatment HTS1, HT was mixed with the wall material at a concentration of 3.06 mg/g while as, the concentration of HT was raised to 14.11 mg/g of wall material in case of HTS2. Because of its high bioactive potential [57], HT was encapsulated at low theoretical loading capacities of 0.30% and 1.41% for HTS1 and HTS2, respectively. Consequently, the amount of HT loaded in HTS2 (0.56%) was significantly ($p \leq 0.05$) higher than in HTS1 (0.14%). The higher concentration of HT in HTS2 results in enhanced packaging of the HT molecules within the chitosan nanocapsules as compared to a less initial concentration of HT used in case of HTS1. Under these circumstances both HTS1 and HTS2 showed very high EE. The EE of HTS1 (77.13%) was significantly ($p \leq 0.05$) higher than HTS2 (56.30%). Various researchers have observed lowering of EE upon increasing the drug load to wall material ratio [6,14].

3.3. Morphology

The morphology of HT nanocapsules analyzed through field emission scanning electron microscopy (FESEM) is presented in Fig. 1. The nanosize of the capsules revealed through DLS measurements is also in coherence with the real time images of the nanocapsules. Ionic gelation of chitosan with sodium sulfate resulted in spherical to irregular shaped nanocapsules. The surface of these nanocapsules showed groves and ridges as compared to the pure HT crystals, which showed smooth sheeted crystal structures. Therefore, there are ample possibilities that the HT crystals are encapsulated in the cavities or the ridges of the nanocapsules. Similar morphology has been reported in ionically gelled chitosan-tripolyphosphate nanoparticles treated with ultrasonication [25]. However, the existence of aggregated nanoparticles is because of their inconsiderable impact on the process of cavitation during the ultrasonication process [60].

3.4. Attenuated total reflectance-Fourier transform infrared spectroscopy

The different materials involved in this research were evaluated through ATR-FTIR analysis for analyzing the functional groups of structural significance (Fig. 2). The stretch in sodium bisulfate at 1027 cm^{-1} corresponds to sulfate ($-\text{SO}_4$) group (Fig. 2a). The stretches at 1650 cm^{-1} to 3500 cm^{-1} correspond to $-\text{OH}$ stretching of hydrogen sulfate ($-\text{HSO}_4$) group. The stretch at 1650 cm^{-1} also corresponds to the hydroxyl ($-\text{OH}$) group of water. In case of HT, the functional region comprising of the aliphatic and aromatic ($-\text{OH}$) groups is exactly super imposable when compared to the ATR-FTIR spectrum of pure water. Therefore, evaluation of HT rich aqueous solutions after extraction of HT from HTS1 and HTS2 were offset for confirmatory studies in this research. For the chitosan polymer, the ATR-FTIR spectrum showed the characteristic ($-\text{OH}$) group at 3350 cm^{-1} (Fig. 2a). The free amino ($-\text{NH}_2$) group of glucosamine was observed at 1027 cm^{-1} to 1214 cm^{-1} . The stretch for Amide I was seen at 1644 cm^{-1} and the Amide III stretch at 1304 cm^{-1} . The carbonyl ($-\text{CO}$) group of the pyranose was observed at 1151 cm^{-1} to 1200 cm^{-1} . The results are in accordance with previous studies on chitosan polymer [61]. The ATR-FTIR spectrum inferences for control, HTS1 and HTS2 did not show any prominent difference in chemistry thereby, showing no prominent molecular differences (Fig. 2b). Therefore, in a multi component system involving chitosan and sodium bisulfate displaying the same functional stretches as in case of HT, the ATR-FTIR spectral analysis can be used for point information only. However, as compared to the pure chitosan polymer, the ($-\text{OH}$) stretch was observed at 3357 cm^{-1} . The stretch of ($-\text{NH}_2$) shifted between 1103 cm^{-1} to 1235 cm^{-1} , which might also include the sulfate ($-\text{SO}_4$) group initially found at 1027 cm^{-1} in case of sodium bisulfate. The stretch for Amide I was observed at 1650 cm^{-1} and the Amide III at

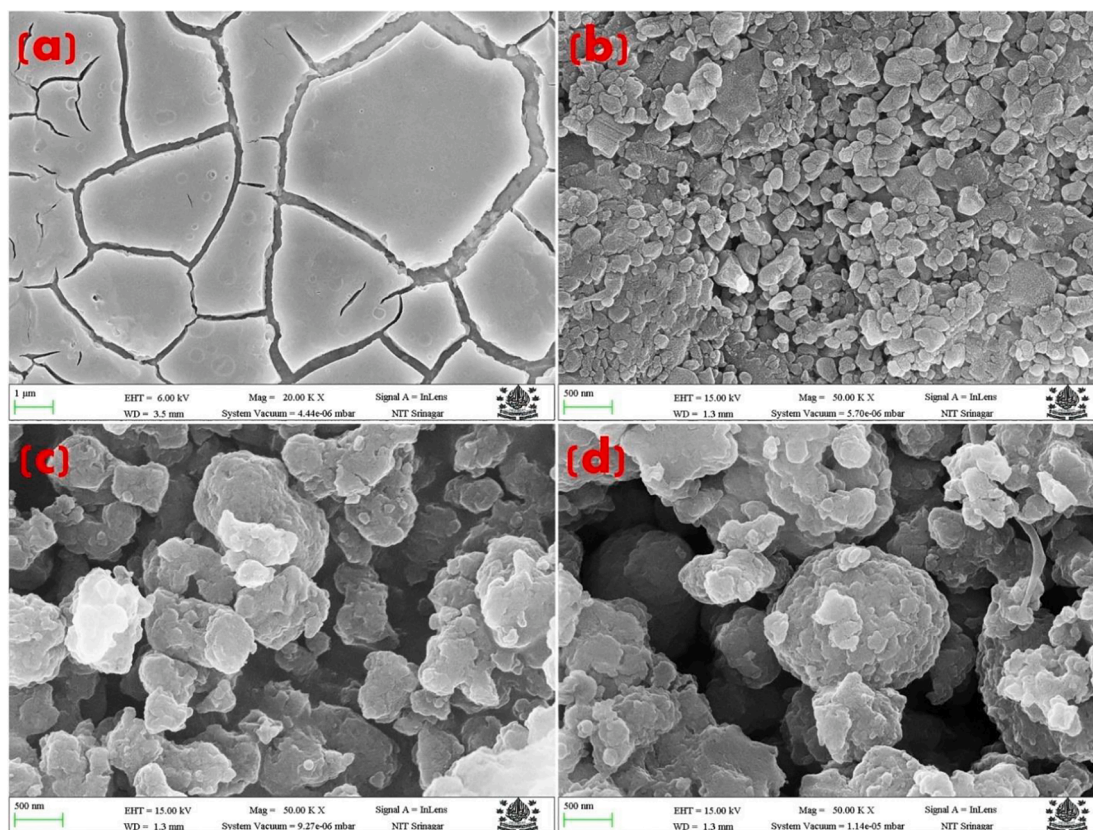


Fig. 1. Field emission scanning electron microscopy (FESEM) images of (a) HT, (b) control nanocapsules, (c) HTS1 nanocapsules, and (d) HTS2 nanocapsules.

1297 cm^{-1} . Meanwhile, the $(-\text{CO})$ group of the pyranose shifted between 1138 cm^{-1} to 1241 cm^{-1} . The major chemical shift was observed between 1138 cm^{-1} to 1241 cm^{-1} of the encapsulated powders that might be due to the formation of gel between the chitosan polymer and sodium bisulfate. Similar results were reported by Jothimani, Sureshkumar, & Venkatachalapathy [29] on chitosan nanoparticles and Du et al. [18] on chitosan-tripolyphosphate nanoparticles encapsulating peptides from egg white.

3.5. X-ray diffraction

The XRD analysis of the individual wall material components and the nanoencapsulated HT powders is presented in Fig. 3. Sodium bisulfate showed the characteristic peaks at the 2θ of 14.68° , 19.48° , and 28.86° . Over the years, research on the XRD pattern of sodium bisulfate has revealed the three characteristic peaks at the 2θ of 12.87° , 17.08° , and around 27° [35,20]. As also reported in our previous research, the crystalline regions of chitosan are observed at the 2θ of $\approx 20^\circ$ and the amorphous regions are observed at the 2θ of $\approx 9^\circ$ with a relative crystallinity of 74.54% [55]. The most prominent diffraction peaks of the ionically crosslinked nanopowder materials were observed at 2θ of 22.66° , 23.64° , 25.58° , 31.86° and 34.06° . Upon the ionic gelation of chitosan with sodium bisulfate, the crystallinity of control, HTS1 and HTS2 nanopowders was recorded as 15.48%, 12.34% and 12.95%, respectively. Therefore, the nanoencapsulated powder materials prepared in the present research were fairly amorphous in nature. Upon ionic gelation, the characteristic chitosan peaks decreased drastically in magnitude. The typical sodium bisulfate peak shifted slightly to the 2θ of 23.64° with prominent increase in intensity. The crystallite size of the encapsulated powders calculated according to the Hall-Williamson analysis was recorded in the range of 20 nm to 27 nm. Reduction of crystallite size in the encapsulated powder with respect to the parent wall materials depicts the tendency to yield nanoparticles through

reduction in the growth of the particle size [45]. chitosan nanoparticles are readily formed through the ionic gelation process [21,13]. Moreover, the acoustic cavitation bubbles formed from intense ultrasound waves also result in reducing the growth of nanoparticles by initiating the polymer chain formation and the subsequent breakage of the resulting chain through the shearing forces resulting from the collapse of the bubbles [33].

3.6. Differential scanning calorimetry

Results of the differential scanning calorimetry (DSC) for the different samples analyzed in this research are presented in Fig. 4. The DSC for sodium bisulfate shows an endothermic peak at 71.02°C that represents its melting behavior. The melting point of sodium bisulfate is around 58.5°C , which is close to the onset of the melting peak. Another endothermic peak for sodium bisulfate at 185.18°C represents the boiling of the compound. At elevated temperatures, sodium bisulfate is decomposed to sodium pyrosulfate ($\text{Na}_2\text{S}_2\text{O}_7$). The two endothermic peaks correspond to respective enthalpy changes (ΔH) of -177.39 Jg^{-1} and -38.18 Jg^{-1} . In case of chitosan, the first endothermic peak (69.35°C) represents the dehydration of the polymer. The glass transition temperature of chitosan was recorded at 149.93°C . The glass transition temperature of chitosan is reported between 140°C and 150°C [17]. This is followed by the exothermic peak (307.23°C) of the material that represents the melting of the polymer followed by decomposition. Chitosan decomposition is characterized by degradation of D-glucosamine and then N-acetyl glucosamine [55]. The dehydration peaks of control (67.07°C), HTS1 (70.68°C) and HTS2 (67.07°C) resemble that of the chitosan polymer. The glass transition temperature of control, HTS1 and HTS2 increased around 191.43°C , which is because of the crosslinking during ionic gelation that reduces the mobility and free volume of the resulting nanoparticles [16]. The final endothermic peaks of control (249.15°C), HTS1 (247.97°C) and HTS2

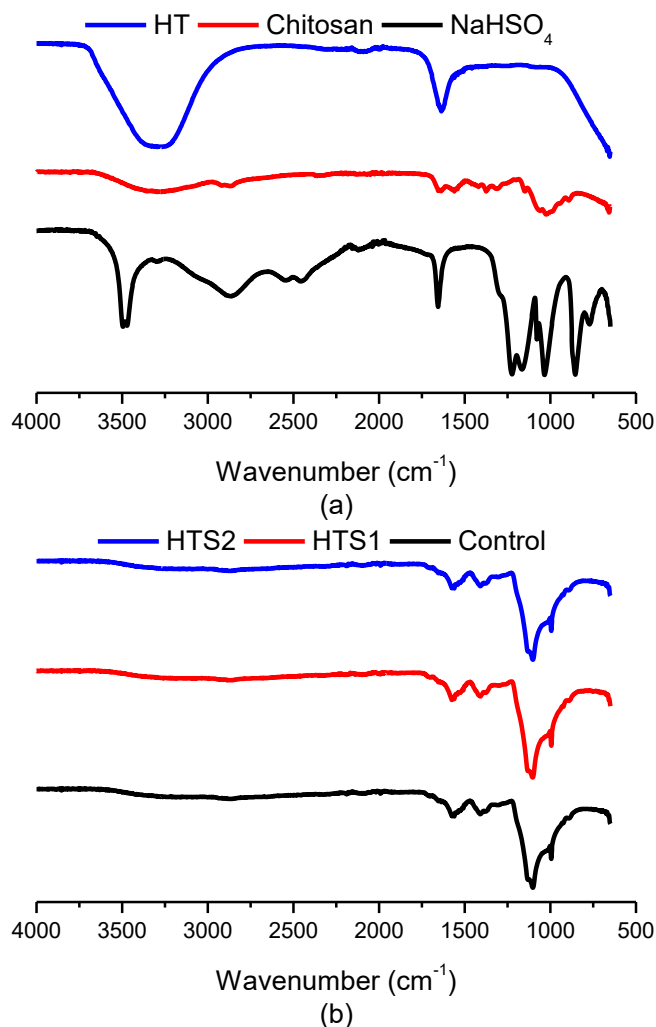


Fig. 2. Attenuated total reflectance-Fourier transform infrared (ATR-FTIR) spectra of (a) HT, schitosan polymer, & sodium bisulfate and (b) control nanocapsules, HTS1, & HTS2.

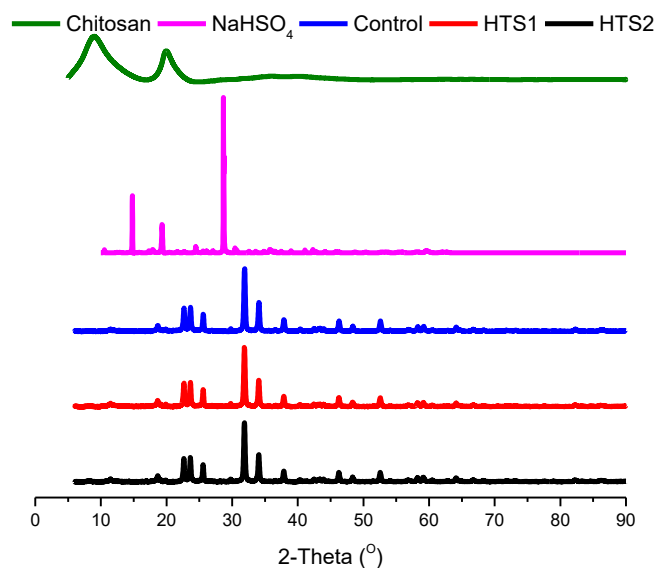


Fig. 3. X-ray diffraction (XRD) diffractograms of of chitosan polymer, NaHSO₄, control nanocapsules, HTS1 and HTS2.

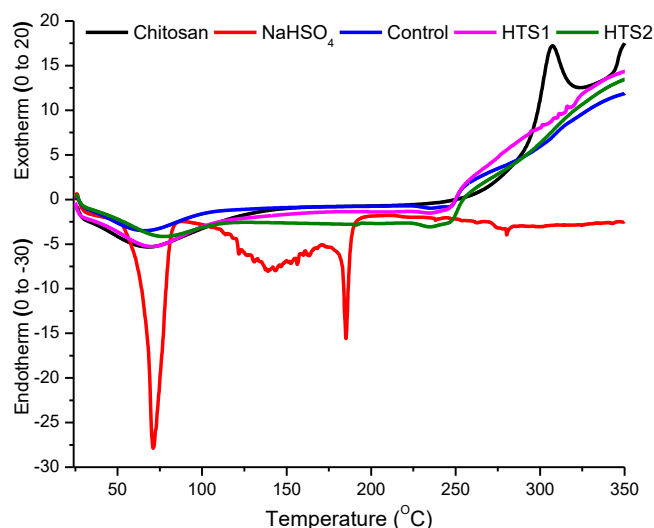


Fig. 4. Differential scanning calorimetry (DSC) of chitosan polymer, NaHSO₄, control nanocapsules, HTS1 and HTS2.

(249.15 °C) represent melting of the samples with corresponding ΔH of -0.16 Jg^{-1} , -2.55 Jg^{-1} and -0.16 Jg^{-1} , respectively. The DSC curves of chitosan polymer, control nanocapsules, HTS1 and HTS2 continuously moving upwards at the end of the melting phases represents the decomposition of these materials upon further rise in temperature. Because very minute amount of HT was incorporated on a percent basis in the nanocapsules, there is no marked difference between the nanocapsules on the basis of the amount of HT incorporated.

3.7. In vitro release behavior

There is a general consensus among scientists that encapsulation safeguards bioactive compound against deleterious reactions inside and outside the biological system [54]. Encapsulation enhances the bioactivity of compounds through improvements in aqueous solubility and absorption upon the delivery at the targeted colonic region of the alimentary canal [53]. As a free molecule, the bioactive potential of HT is not completely realized owing to its low bioavailability. As a result, only a small concentration of HT is found in the blood stream post consumption [41]. Upon consumption, an extremely small maximum plasma concentration (4.4 ng/mL) of free HT is reached within just 15 min [42]. This necessitates the encapsulation of free HT for preventing the molecule from being exposed to the harsh gastrointestinal acid and enzymatic conditions as well as releasing it at the intestinal absorption sites.

HT nanoencapsulated in the form of HTS1 and HTS2 were subjected to simulated gastrointestinal release studies and the results are provided in Fig. 5. While subjecting the nanoencapsulated HT to simulated gastric digestion (SGD), its release was monitored after 30 min and 60 min. The release of HT from the nanocapsules during simulated intestinal digestion (SID) was monitored hourly for 2 h. The release of HT after 30 min of SGD in HTS1 and HTS2 was 28.32% and 10.90%, respectively. This amount of HT is probably the non-encapsulated HT present on the surface of the capsules. As the SGD is continued to 1 h, there was significantly ($p \leq 0.05$) more release of HT from both HTS1 (37.80%) and HTS2 (38.55%), considering the initial releasing point of the two samples. The release of a lesser amount of HT from HTS1 during SGD is probably due to the small amount of HT encapsulated in it as compared to HTS2. After 1 h of SID, the release of HT from HTS2 reached up to 60.00% and HTS1 up to 42.02%. Besides, the cumulative release of HT from 42.02% to 58.89% after 2 h of SID ensures a delayed and sustained release of HT from HTS2. While as, it was 60.00% to 67.12% in case of HTS1. At the end of SID, HTS2 delivered up to 67.12% and HTS1 up to

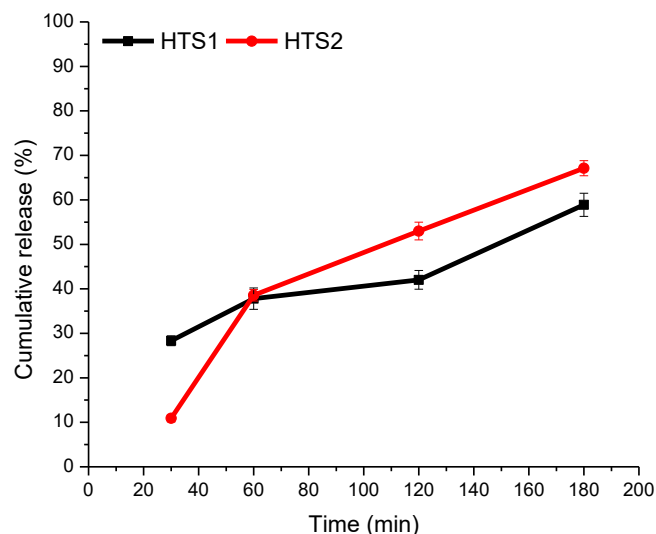


Fig. 5. In vitro release of HT from HTS1 and HTS2 post simulated gastric digestion (0–60 min) and simulated intestinal digestion (60–180 min).

58.89% of HT. Therefore, the HT nanocapsules were able to retain most of the HT after the SGD for possible uptake at the intestinal and colonic sites towards the end of the digestion process.

3.8. Antioxidant potential

The antioxidant potential of nanoencapsulated HT was carried out against the free HT after subjecting them to *in vitro* simulated gastrointestinal digestion (SGID). The antioxidant potential analyzed through DPPH radical scavenging activity and lipid peroxidation inhibition (LPI) is presented in Fig. 6. The DPPH radical scavenging activity is often used for relatively rapid evaluation of the antioxidant activity. In DPPH radical scavenging activity, the radical accepts an electron or hydrogen radical to become a stable diamagnetic molecule with corresponding change in color. The concentration of free HT used in this study corresponds to the encapsulation efficiency of HTS2. This confirmed the validity and requirement of the nanoencapsulation process for the bioavailability of HT post SGID. The DPPH radical scavenging activity of HTS2 (71.59%) was significantly ($p \leq 0.05$) higher than both the HTS1 (13.10%) and the free HT (3.36%). In fact, the free HT showed the lowest ($p \leq 0.05$) DPPH radical scavenging activity. The DPPH radical scavenging activity of HT is attributed to its catechol nucleus [57], which could be reduced due to possible destruction of HT in the acidic

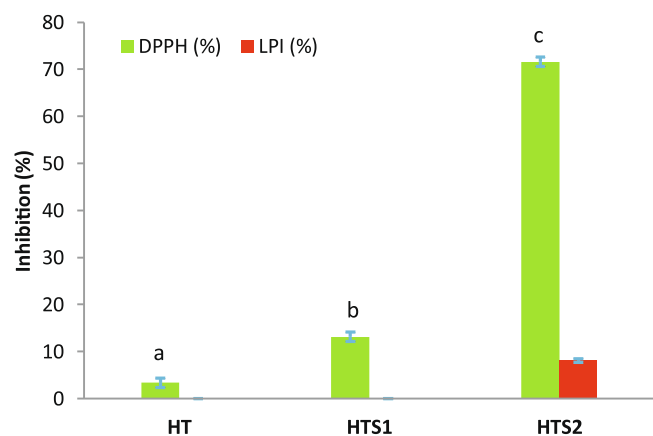


Fig. 6. Antioxidant properties (DPPH radical scavenging activity and lipid peroxidation inhibition) of nanoencapsulated HT.

and enzymatic conditions during the SGID. On the other hand, the LPI evaluates the free radical mediated antioxidant potential by monitoring the inhibition of a possible chain initiation, propagation and/or termination of linoleic acid peroxidation [39]. The LPI was undetectable for the free HT and HTS1. However, HTS2 (8.07%) showed small amount of LPI. Therefore, it is evident from the results that LPI might also depend on the concentration of the available bioactive compound. The analysis of radical scavenging activities using different solvent media and nature of chemicals reveal the antioxidant potential in the heterogeneous biological system through a complex set of possible variations in the interactive mechanisms involved during the reaction of the radicals with the biological system [40,26]. Over all, these results confirm the need and importance of the nanoencapsulation process for HT delivery and achieving a substantial amount of antioxidant activity at a very low concentration.

3.9. Antiproliferative properties

Antiproliferative properties of the nanoencapsulated HT against adenocarcinomic human alveolar epithelial cells (A549) and human breast cancer cells (MDA-MB-231) is presented in the form of IC_{50} values (Fig. 7) over a period of 72 h. The alveolar epithelial cells line the lung alveoli and play a key role in carrying out the gaseous exchange process inside the lungs [52]. In the present investigation, free HT showed high antiproliferative activity against A549 cell line over the 72 HTP. The IC_{50} values for HT reduced from 230.60 μ M to 149.36 μ M over the entire study (Fig. 7a). However, the nanoencapsulated HT showed significantly ($p \leq 0.05$) higher antiproliferative properties than the free HT over the complete 72 HTP. For HTS1, the IC_{50} values reduced from 199.18 μ M to 60.74 μ M, while in case of HTS2, the IC_{50} values reduced from 125.28 μ M to 56.31 μ M, over the 72 HTP. The antiproliferative effect of HTS2 on A549 cell line was higher than HTS1 for 24 HTP and did not differ significantly over the next two time periods. To the best of our knowledge, there are no reports on antiproliferative properties of nanoencapsulated HT against the A549 cell line. However, Calderon-Montano et al. [10] reported an IC_{50} value of 147 ± 16.5 μ M for free HT against the A549 cell line, which is consistent with the present research.

The triple negative MDA-MB-231 is a highly aggressive form of breast cancer, which lacks oestrogen and progesterone receptor expressions, as well as the human epidermal growth factor receptor 2 amplification [36,12]. Therefore, the MDA-MB-231 cell line is particularly employed to analyze the activity of different active compounds with potential antiproliferative properties. The IC_{50} value of free HT against MDA-MB-231 cell line increased from 107.17 μ M to 183.65 μ M during the 72 HTP (Fig. 7b), which depicts the reduction in the effectiveness of free HT with respect to time. However, the IC_{50} value for HTS2 was significantly higher than HTS1 throughout the 72 HTP. This depicts the dose dependent relationship of the antiproliferative activity as well as the application of nanoencapsulation on the effectiveness of HT against the MDA-MB-231 cell line. To the best of our knowledge, there are no reports on antiproliferative properties of nanoencapsulated HT against the MDA-MB-231 cell line. However, Benot-Dominguez et al. [5] demonstrated the antiproliferative effect of olive leaf extract containing HT against MDA-MB-231. Tavolaro, Catalano, & Tavolaro [51] also showed the antiproliferative activity of extra virgin olive oil (a source of HT) against MDA-MB-231 cell line. The antioxidant potential (DPPH radical scavenging activity) showed a negative correlation with A549 ($R = -0.82$) and MDA-MB-231 ($R = -0.71$). This depicts that upon increase in the antioxidant activities, the concentration required for IC_{50} is decreased.

4. Conclusion

In conclusion, ionic gelation of chitosan polymer with sodium bisulfate using ultrasonication in tandem produced spherical to irregular

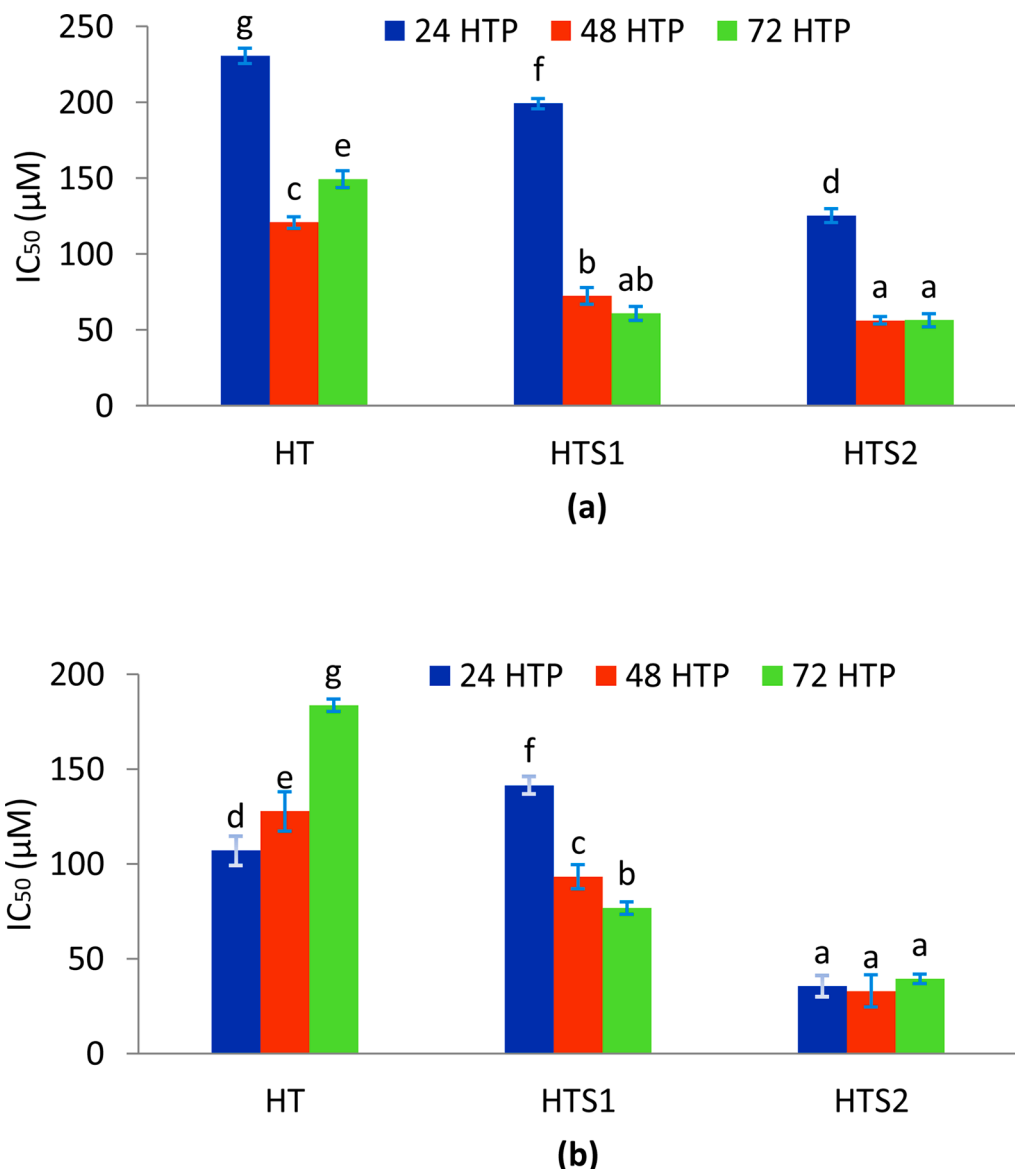


Fig. 7. Antiproliferative properties of the nanoencapsulated HT against (a) adenocarcinomic human alveolar epithelial cells (A549) and (b) human breast cancer cells (MDA-MB-231).

shaped amorphous nanocapsules that encapsulated HT. The nanoencapsulated HT was protected against the acidic and enzymatic conditions during the gastrointestinal simulations to release the free HT slowly and particularly in the colonic site, where its absorption mainly takes place. The nanoencapsulated HT (HTS2) exhibited better antioxidant and antiproliferative properties than the free HT in a dose dependent manner. The nanoencapsulated HT (HTS2) could be utilized in various food formulations and other medical applications as a preventive medicine. The prepared nanocapsules could be utilized for the oral delivery of sensitive bioactives and drug compounds in various food formulations and other medical applications.

5. Author statement

Touseef Ahmed Wani performed the experiments, drafted the manuscript and revised it. F.A. Masoodi conceptualized and supervised the research. Rehana Akhter assisted in laboratory experimentation. Towseef Akram assisted in antiproliferative analysis, Adil Gani assisted in laboratory experimentation, Nadeem Shabir assisted in antiproliferative analysis.

Declaration of Competing Interest

The authors declare that they have no known competing financial interests or personal relationships that could have appeared to influence the work reported in this paper.

Acknowledgements

Touseef Ahmed Wani acknowledges the Council of Scientific & Industrial Research (CSIR) New Delhi, India for providing the Senior Research Fellowship (SRF) grant (09/251/(0070)/2K17).

References

- [1] K. Abstiens, A.M. Goepferich, Microfluidic manufacturing improves polydispersity of multicomponent polymeric nanoparticles, *J. Drug Delivery Sci. Technol.* 49 (2019) 433–439.
- [2] M. Ahmad, A. Gani, Ultrasonicated resveratrol loaded starch nanocapsules: Characterization, bioactivity and release behaviour under in-vitro digestion, *Carbohydr. Polym.* 251 (2021) 117111, <https://doi.org/10.1016/j.carbpol.2020.117111>.

- [3] M. Ahmad, P. Mudgil, A. Gani, F. Hamed, F.A. Masoodi, S. Maqsood, Nano-encapsulation of catechin in starch nanoparticles: Characterization, release behavior and bioactivity retention during simulated in-vitro digestion, *Food Chem.* 270 (2019) 95–104.
- [4] S. Anandhakumar, G. Krishnamoorthy, K.M. Ramkumar, A.M. Raichur, Preparation of collagen peptide functionalized chitosan nanoparticles by ionic gelation method: An effective carrier system for encapsulation and release of doxorubicin for cancer drug delivery, *Mater. Sci. Eng., C* 70 (2017) 378–385.
- [5] R. Benot-Dominguez, M.G. Tupone, V. Castelli, M. d'Angelo, E. Benedetti, M. Quintiliani, B. Cinque, I.M. Forte, M.G. Cifone, R. Ippoliti, B. Barboni, A. Giordano, A. Cimini, Olive leaf extract impairs mitochondria by pro-oxidant activity in MDA-MB-231 and OVCAR-3 cancer cells, *Biomed. Pharmacother.* 134 (2021) 111139, <https://doi.org/10.1016/j.biopha.2020.111139>.
- [6] A. Bermúdez-Oria, G. Rodríguez-Gutiérrez, F. Rubio-Senent, A. Lama-Muñoz, J. Fernández-Bolaños, Complexation of hydroxytyrosol and 3,4-dihydroxyphenylglycol with pectin and their potential use for colon targeting, *Carbohydr. Polym.* 163 (2017) 292–300.
- [7] A. Berthold, K. Cremer, J. Kreuter, Preparation and characterization of chitosan microspheres as drug carrier for prednisolone sodium phosphate as model for antiinflammatory drugs, *J. Control. Release* 39 (1) (1996) 17–25.
- [8] S. Bhardwaj, N.K. Bhardwaj, Y.S. Negi, Effect of degree of deacetylation of chitosan on its performance as surface application chemical for paper-based packaging, *Cellulose* 27 (9) (2020) 5337–5352.
- [9] C. Bonechi, A. Donati, G. Tamasi, A. Pardini, H. Rostom, G. Leone, S. Lamponi, M. Consumi, A. Magnani, C. Rossi, Chemical characterization of liposomes containing nutraceutical compounds: Tyrosol, hydroxytyrosol and oleuropein, *Biophys. Chem.* 246 (2019) 25–34.
- [10] J.M. Calderón-Montaña, A. Madrona, E. Burgos-Morón, M.L. Orta, S. Mateos, J. L. Espartero, M. López-Lázaro, Selective cytotoxic activity of new lipophilic hydroxytyrosol alkyl ether derivatives, *J. Agric. Food. Chem.* 61 (21) (2013) 5046–5053.
- [11] M.D. Chatzidakis, N. Arik, J. Monteil, V. Papadimitriou, F. Leal-Calderon, A. Xenakis, Microemulsion versus emulsion as effective carrier of hydroxytyrosol, *Colloids Surf., B* 137 (2016) 146–151.
- [12] K.J. Chavez, S.V. Garimella, S. Lipkowitz, J. Eng-Wong, J.A. Zujewski, Triple negative breast cancer cell lines: One tool in the search for better treatment of triple negative breast cancer, *Breast Disease* 32 (1–2) (2011) 35–48.
- [13] Y. Ciro, J. Rojas, A.L. Di Virgilio, M.J. Alhaji, G.A. Carabali, C.H. Salamanca, Production, physicochemical characterization, and anticancer activity of methotrexate-loaded phytic acid-chitosan nanoparticles on HT-29 human colon adenocarcinoma cells, *Carbohydr. Polym.* 243 (2020) 116436, <https://doi.org/10.1016/j.carbpol.2020.116436>.
- [14] B.D. Couto, R.N. da Costa, W.C. Laurindo, H.M. da Silva, C.R. da Silva, J.S.D. R. Coimbra, A.B. Mageste, S. de Cássia Dias, L.J.B. Santos, Characterization, technological properties, and encapsulation efficiency of self-assembled β -lactoglobulin nanostructures, *Food Chem.* 356 (2021) 129719.
- [15] M.-C. López de las Hazas, C. Piñol, A. Macià, M.-J. Motilva, Hydroxytyrosol and the colonic metabolites derived from virgin olive oil intake induce cell cycle arrest and apoptosis in colon cancer cells, *J. Agric. Food. Chem.* 65 (31) (2017) 6467–6476.
- [16] A. Dereymaker, G. Van Den Mooter, The Peculiar Behavior of the Glass Transition Temperature of Amorphous Drug-Polymer Films Coated on Inert Sugar Spheres, *J. Pharm. Sci.* 104 (5) (2015) 1759–1766.
- [17] Y. Dong, Y. Ruan, H. Wang, Y. Zhao, D. Bi, Studies on Glass Transition Temperature of Chitosan with Four Techniques, *J. Appl. Polym. Sci.* 93 (4) (2004) 1553–1558.
- [18] Z. Du, J. Liu, T. Zhang, Y. Yu, Y. Zhang, J. Zhai, H. Huang, S. Wei, L. Ding, B. Liu, A study on the preparation of chitosan-tripolyphosphate nanoparticles and its entrapment mechanism for egg white derived peptides, *Food Chem.* 286 (2019) 530–536.
- [19] EFSA, EFSA panel on dietetic products, nutrition and allergies (NDA); Scientific opinion on the substantiation of health claims related to polyphenols in olive and protection of LDL particles from oxidative damage (ID 1333, 1638, 1639, 1696, 2865), maintenance of normal blood HDL-cholesterol concentrations (ID 1639), maintenance of normal blood pressure (ID 3781), anti-inflammatory properties (ID 1882), contributes to the upper respiratory tract health (ID 3468), can help to maintain a normal function of gastrointestinal tract (3779), and contributes to body defences against external agents (ID 3467) pursuant to Article 13(1) of Regulation (EC) No 1924/2006, *EFSA J.* 9 (2011) 25.
- [20] Y. Ennaciri, M. Bettach, H. El Alaoui-Belghiti, Conversion of Moroccan phosphogypsum waste into nano-calcium fluoride and sodium hydrogen sulfate monohydrate, *J. Mater. Cycles Waste Manage.* 22 (2020) 2039–2047.
- [21] W. Fan, W. Yan, Z. Xu, H. Ni, Formation mechanism of monodisperse, low molecular weight chitosan nanoparticles by ionic gelation technique, *Colloids Surf., B* 90 (2012) 21–27.
- [22] R. Feng, L. Wang, P. Zhou, Z. Luo, X. Li, L. Gao, Development of the pH responsive chitosan-alginate based microgel for encapsulation of *Jughans regia* L. polyphenols under simulated gastrointestinal digestion in vitro, *Carbohydr. Polym.* 250 (2020) 116917.
- [23] L. Flaiz, M. Freire, S. Cofrades, R. Mateos, J. Weiss, F. Jimenez-Colmenero, R. C. Bou, L. Flaiz, A. Garcimartin, J. Benedi, F.J. Sanchez-Muniz, R. Olivero-David, Comparison of simple, double and gelled double emulsions of hydroxytyrosol and n-3 fatty acid delivery system, *Food Chem.* 54 (2016) 49–57.
- [24] C. Flores, M. Lopez, N. Tabary, C. Neut, F. Chai, D. Betbeder, C. Herkt, F. Cazaux, V. Gaucher, B. Martel, N. Blanchemain, Preparation and characterization of novel chitosan and β -cyclodextrin polymer sponges for wound dressing applications, *Carbohydr. Polym.* 173 (2017) 535–546.
- [25] A. Floris, M.C. Meloni, F. Lai, F. Marongiu, A.M. Maccioni, C. Sinico, Cavitation effect on chitosan nanoparticle size: A possible approach to protect drugs from ultrasonic stress, *Carbohydr. Polym.* 94 (2013) 619–625.
- [26] M.N. Franco, T. Galeano-Díaz, Ó. López, J.G. Fernández-Bolaños, J. Sánchez, C. De Miguel, M.V. Gil, D. Martín-Vertedor, Phenolic compounds and antioxidant capacity of virgin olive oil, *Food Chem.* 163 (2014) 289–298.
- [27] T. Ito, T. Takami, Y. Uchida, Y. Murakami, Chitosan gel sheet containing drug carriers with controllable drug-release properties, *Colloids Surf., B* 163 (2018) 257–265.
- [28] B. Joshi, J. Kaur, E. Khan, A. Kumar, A. Joshi, Ultrasonic atomizer driven development of doxorubicin-chitosan nanoparticles as anticancer therapeutics: Evaluation of anionic cross-linkers, *J. Drug Delivery Sci. Technol.* 57 (2020) 101618.
- [29] B. Jothimani, S. Sureshkumar, B. Venkatachalapathy, Hydrophobic structural modification of chitosan and its impact on nanoparticle synthesis - a physicochemical study, *Carbohydr. Polym.* 173 (2017) 714–720.
- [30] S.H. Kim, Y.C. Ryu, H.-M.-D. Wang, B.H. Hwang, Optimally Fabricated Chitosan Particles Containing Ovalbumin Induced Cellular and Humoral Immunity in Immunized Mice, *Biotechnol. Bioprocess Eng.* 25 (2020) 681–689.
- [31] Prasanth B. Koppolu, S.G. Smith, S. Ravindranathan, S. Jayanthi, T.K. Suresh Kumar, D.A. Zaharoff, Controlling chitosan-based encapsulation for protein and vaccine delivery, *Biomaterials* 35 (14) (2014) 4382–4389.
- [32] S. Kumari, S.H.K. Annamareddy, S. Abanti, P.K. Rath, Physicochemical properties and characterization of chitosan synthesized from fish scales, crab and shrimp shells, *Int. J. Biol. Macromol.* 104 (2017) 1697–1705.
- [33] T.S.H. Leong, G.J.O. Martin, M. Ashokkumar, Ultrasonic encapsulation - A review, *Ultrason. Sonochem.* 35 (2017) 605–614.
- [34] J. Li, Q. Zhao, Chitosan microspheres loading whole cell protein antigen of *Helicobacter pylori*: Preparation and in vitro release characteristics, *Chin. J. Tissue Eng. Res.* 53 (2015) 3334–3338.
- [35] H. Liu, C. Xiang, B. Yang, S. Yang, Q. Li, Microwave intensified synthesis of regular shaped sodium bisulfate crystal, *Chem. Eng. Process. Process Intensification* 95 (2015) 208–213.
- [36] H. Liu, C. Zang, M.H. Fenner, K. Possinger, E. Elstner, PPARgamma ligands and ATRA inhibit the invasion of human breast cancer cells in vitro, *Breast Cancer Res. Treat.* 79 (2003) 63–74.
- [37] B. Matthus, Antioxidant activity of extracts obtained from residues of different oilseeds, *J. Agric. Food. Chem.* 5 (2002) 3444–3452.
- [38] D.J. McClements, Y. Li, Structured emulsion-based delivery systems: Controlling the digestion and release of lipophilic food components, *Adv. Colloid Interface Sci.* 159 (2010) 213–228.
- [39] E. Niki, Lipid peroxidation: Physiological levels and dual biological effects, *Free Radical Biol. Med.* 47 (2009) 469–484.
- [40] E. Niki, Y. Yoshida, Y. Saito, N. Noguchi, Lipid peroxidation: Mechanisms, inhibition, and biological effects, *Biochem. Biophys. Res. Commun.* 338 (2005) 668–676.
- [41] M.I. Orozco-Solano, C. Ferreira-Vera, F. Priego-Capote, M.D.L. de Castro, Automated method for determination of olive oil phenols and metabolites in human plasma and application in intervention studies, *J. Chromatogr. A* 1258 (2012) 108–116.
- [42] A. Pastor, J. Rodríguez-Morató, E. Olesti, M. Pujadas, C. Pérez-Maná, O. Khymenets, M. Fitó, M.I. Covas, R. Solá, M.J. Motilva, M. Farré, R. de la Torre, Analysis of free hydroxytyrosol in human plasma following the administration of olive oil, *J. Chromatogr. A* 1437 (2016) 183–190.
- [43] F. Paulo, L. Santos, Inclusion of hydroxytyrosol in ethyl cellulose microparticles: *In vitro* release studies under digestion conditions, *Food Hydrocolloids* 84 (2018) 104–116.
- [44] A.C.S.N. Pessoa, C.C. Sipoli, L.G. de la Torre, Effects of diffusion and mixing pattern on microfluidic-assisted synthesis of chitosan/ATP nanoparticles, *Lab Chip* 17 (2017) 2281–2293.
- [45] T. Preethi, B. Abarna, G.R. Rajarajeswari, Influence of chitosan-PEG binary template on the crystallite characteristics of sol-gel synthesized mesoporous nanotitanaphoto catalyst, *Appl. Surf. Sci.* 317 (2014) 90–97.
- [46] N. Sawtarie, Y. Cai, Y. Lapitsky, Preparation of chitosan/tripolyphosphate nanoparticles with highly tunable size and low polydispersity, *Colloids Surf. B-Biointerf.* 157 (2017) 110–117.
- [47] Y. Shao, B. Zhu, J. Li, X. Liu, X. Tan, X. Yang, Novel chitosan microsphere-templated microcapsules suitable for spontaneous loading of heparin, *Mater. Sci. Eng., C* 29 (2009) 936–941.
- [48] K.R. Shouair, N. El-Desouky, M.M. Rashad, M.K. Ahmed, I. Janowska, M. El-Kemary, Chitosan based-nanoparticles and nanocapsules: Overview, physicochemical features, applications of a nanofibrous scaffold, and bioprinting, *Int. J. Biol. Macromol.* 167 (2021) 1176–1197.
- [49] E.K. Silva, G.L. Zabet, A.A.C.T. Hijo, M.A.A. Meireles, Ultrasonic: Advances for Food Processing and Preservation, in: D. Bermudez-Aguirre (Ed.), *Encapsulation of Bioactive Compounds Using Ultrasonic Technology*, Academic Press, New York, 2017, pp. 323–350.
- [50] T. Songkroh, H. Xie, W. Yu, X. Liu, G. Sun, X. Xu, X. Ma, Injectable in situ forming chitosan-based hydrogels for curcumin delivery, *Macromol. Res.* 23 (2015) 53–59.
- [51] P. Tavaloro, S. Catalano, A. Tavaloro, Anticancer activity modulation of an innovative solid formulation of extra virgin olive oil by cultured zeolite scaffolds, *Food Chem. Toxicol.* 124 (2019) 139–150.
- [52] R. Wang, D.-Z. Sun, C.-Q. Song, Y.-M. Xu, W. Liu, X.-S. Dong, Eukaryotic translation initiation factor 2 subunit α (eIF2 α) inhibitor salubrinal attenuates paraquat-induced human lung epithelial-like A549 cell apoptosis by regulating the PERK-eIF2 α signaling pathway, *Toxicol. In Vitro* 46 (2018) 58–65.

- [53] T.A. Wani, A. Gani, S.M. Wani, F.A. Masoodi, I.A. Wani, N. Baba, M.A. Shagoo, Suitability of Different Food Grade Materials for the Encapsulation of Some Functional Foods Well Reported for Their Advantages and Susceptibility, *Crit. Rev. Food Sci. Nutr.* 56 (2016) 2431–2454.
- [54] T.A. Wani, F.A. Masoodi, I.A. Wani, The possible nomenclature of encapsulated products, *Food Chem.* 234 (2017) 119–120.
- [55] T.A. Wani, F.A. Masoodi, R. Akhter, F.A. Sofi, Techno-functional characterization of chitosan nanoparticles prepared through planetary ball milling, *Int. J. Biol. Macromol.* 154 (2020) 166–172.
- [56] T.A. Wani, F.A. Masoodi, W.N. Baba, M. Ahmad, N. Rahmanian, S.M. Jafari, Nanoencapsulation of agrochemicals, fertilizers, and pesticides for improved plant production, in: S.M. Jafari (Ed.), *Advances in phytonanotechnology: From synthesis to application*, Academic Press, New York, 2018, pp. 279–298.
- [57] T.A. Wani, F.A. Masoodi, A. Gani, W.N. Baba, N. Rahmanian, R. Akhter, I.A. Wani, M. Ahmad, Olive oil and its principal bioactive compound: Hydroxytyrosol - A review of the recent literature, *Trends Food Sci. Technol.* 77 (2018) 77–90.
- [58] T.A. Wani, F.A. Masoodi, R. Akhter, Preparation and characterization of chitosan flake and chitosan nanopowder gels: A comparative study of rheological, thermal and morphological perspectives, *LWT - Food Sci. Technol.* 148 (2021) 111771.
- [59] J.R. Wright, H.D. Colby, P.R. Miles, Cytosolic factors which affect microsomal lipid peroxidation in lung and liver, *Archeol. Biochem. Biophys.* 206 (1981) 294–304.
- [60] K. Zhang, Y. Xu, L. Lu, C. Shi, Y. Huang, Z. Mao, C. Duan, X. Ren, Y. Guo, C. Huang, Hydrodynamic cavitation: A feasible approach to intensify the emulsion cross-linking process for chitosan nanoparticle synthesis, *Ultrason. Sonochem.* 74 (2021) 105551.
- [61] W. Zhang, J. Zhang, Q. Jiang, W. Xia, Physicochemical and structural characteristics of chitosan nanopowders prepared by ultrafine milling, *Carbohydr. Polym.* 87 (2012) 309–313.
- [62] H. Zubair, A. Bhardwaj, A. Ahmad, S.K. Srivastava, M.A. Khan, G.K. Patel, S. Singh, A.P. Singh, Hydroxytyrosol induces apoptosis and cell cycle arrest and suppresses multiple oncogenic signaling pathways in prostate cancer cells, *Nutr. Cancer* 69 (2017) 932–942.